Functional Materials Letters
Vol. 11, No. 1 (2018) 1850008 (5 pages)

DOI: 10.1142/S179360471850008X

World Scientific
www.worldscientific.com

Low temperature oxidation synthesis of carbon encapsulated Cr_2O_3 nanocrystals and its lithium storage performance

Yun Zhou*,‡, Boyang Liu*,§, Yingfeng Shao†, Chunhua Fan*, Runhua Fan*
and Bosheng Wen*

*College of Ocean Science and Engineering
Shanghai Maritime University, Shanghai 201306, P. R. China

†State Key Laboratory of Nonlinear Mechanics
Institute of Mechanics, Beijing 100190, P. R. China
‡yunzhou@shmtu.edu.cn
§byliu@shmtu.edu.cn

Received 20 September 2017; Accepted 12 December 2017; Published 11 January 2018

A highly efficient and convenient strategy is developed for the one-step *in-situ* synthesis of carbon encapsulated Cr_2O_3 nanocrystals with core-shell structure (Cr_2O_3@C). The explosive reaction of chromocene with ammonium persulfate in an autoclave at 200°C is crucial for the formation of this nanostructure. The Cr_2O_3 nanocrystals have a diameter of 5 to 20 nm, which are entirely encapsulated by the amorphous carbon shell. The Cr_2O_3@C anode can retain a stable reversible capacity of 397 mAh g^{-1} after 50 cycles at a current density of 119 mA g^{-1}.

Keywords: Carbon encapsulated Cr_2O_3 nanocrystals; core-shell; explosive reaction; lithium-ion battery.

Lithium-ion batteries (LIBs) have been widely used in consumer electronics and vehicles because of their advantages of high energy and power density, long service life, low cost and environmental friendliness.[1] The energy storage ability of LIBs strongly depends on the electrode material and its microstructure. Therefore, in the past decade, many efforts have been devoted to the exploration of novel anode materials with a high specific capacity to replace the low-capacity graphite. Many transition metal oxides with unique structure and favorable physicochemical property have been intensively studied as alternate anodes in LIBs.[2] However, low conductivity, large volume change and sluggish kinetics associated with the lithium ions insertion/extraction of these materials result in fast capacity fading and unsatisfactory cycling performance.[3] To alleviate these problems, various types of nanocrystalline materials are used instead to decrease the lithium ion diffusion length, thereby improving the capacity and rate performance.[4] Otherwise, the addition of carbonaceous substances can further enhance the conductivity of the electrode materials and suppress the volume expansion.[5] Thus, carbon encapsulated nanocrystals with core-shell structure are regarded as promising candidates for high-performance LIBs because of their stable structure, excellent property, and acceptable price.[6]

Some general synthesis strategies with a stepwise process have been developed due to the different formation routes for carbon shell and the inner cores. Chemical vapor deposition can be utilized to form a carbon shell on the pre-prepared nanocrystals through the decomposition of the organic precursor at above 600°C.[7] Carbon shell can also be obtained by the preliminary encapsulation by polymer at a low temperature and then followed by a carbonization via thermal pyrolysis at high temperature.[8] Hydrothermal method is extensively carried out in an autoclave using aqueous glucose/sucrose solution. The polymerization and carbonization of these saccharides can simply produce carbon shell at a low temperature of 140–200°C, and some core–shell structure can simultaneously *in-situ* form.[9] But these methods have notable limitations in the aspects of multistep and complicated procedures, large energy consumption (high carbonization temperature), specific facilities and long synthesis time. Thus, it is still worthy to develop simple, efficient and scalable synthesis techniques.

Recently, we have synthesized a dozen of carbon encapsulated metal oxide/sulfide nanocrystals with core–shell

§Corresponding author.

structure by the explosive reaction of metal π-complex with oxidizing agent in an autoclave.[10–12] The synthesis finishes in 30 min and the temperature is as low as 200°C. There is no need to consider the atmosphere in the reactor and only a pressure vessel is enough for the whole process rather than other complicated equipment. The large-scale production in quantity of tens of grams is also promising. Moreover, it is a universal synthesis method for various carbon encapsulated nanocrystals.

Cr_2O_3 has a large theoretical capacity of 1058 mAh g^{-1} and relatively low lithium insertion potential compared with other metal oxides.[13] But pristine Cr_2O_3 exhibits a poor cycling performance probably owing to the huge volume change and the formation of unstable solid electrolyte interphase (SEI) during charge/discharge process.[14] It is proved that carbon incorporation can overcome these shortcomings and improve the cycling stability.[15] Herein, carbon encapsulated Cr_2O_3 nanocrystals with core-shell structure (Cr_2O_3@C) is simply and efficiently achieved by our synthesis method via the reaction of chromocene ($(C_5H_5)_2Cr$, Cp_2Cr) with ammonium persulfate ($(NH_4)_2S_2O_8$). The electrochemical properties of the Cr_2O_3@C anode for LIBs are also measured.

About 10 mmol of Cp_2Cr and 20 mmol of $(NH_4)_2S_2O_8$ were placed into a 50-mL autoclave, which was heated at 200°C for 30 min with a rotational speed of 50 rpm. After that, the as-prepared powder was rinsed in deionized water and air-dried, finally leaving behind the Cr_2O_3@C. It should be pointed out that no solvent was used in this process, which is distinctly different from the hydrothermal route.

Phase characterization was investigated by X-ray diffraction (XRD) using a PANalytical diffractometer with Cu Kα radiation. Micro Raman spectrum was analyzed by a Bruker Raman spectrometer with a 633 nm excitation. The microstructure and composition were examined by the scanning electron microscope (SEM, JEOL 7500F) and transmission electron microscope (TEM, JEOL 2010) equipped with an X-ray energy-dispersive spectroscope (EDS, EDAX). Differential scanning calorimetric (DSC) and thermogravimetric (TG) studies were performed in air on a Netzsch STA 449F3 at a scan rate of 10°C min^{-1}.

The Cr_2O_3@C was mixed with acetylene black and polyvinyldifluoride in N-methyl-2-pyrrolidone in a weight ratio of 80:10:10. The as-prepared homogeneous slurry was pasted on copper foil and subsequently dried in a vacuum oven at 120°C. In the coin cell battery, lithium foil and the Celgard 2400 microporous polypropylene film serve as the counter electrode and separator, respectively. The 1.0 M $LiPF_6$ in a 1:1 (v/v) mixture solvent of ethylene carbonate and dimethyl carbonate was used as the electrolyte. The galvanostatic charge/discharge performance of the cells was recorded on a Neware battery testing system between 0.05 and 3 V with different current density. The cyclic voltammogram (CV) was performed on a CHI 630A electrochemical workstation within a cut-off voltage of 0.01–3.0 V and at a scan rate of 0.1 mV s^{-1}.

The as-prepared black powder is mainly composed of $(NH_4)_2SO_4$ and Cr_2O_3 according to the XRD pattern in Fig. 1(a). The $(NH_4)_2SO_4$ is one of the typical decomposition product of $(NH_4)_2S_2O_8$ at about 200°C.[16] The sensitive Cp_2Cr is easily oxidized to Cr_2O_3 at this temperature. After washing out $(NH_4)_2SO_4$, the Cr_2O_3 phase is dominant, while a small amount of Cr_2S_3 can also be indexed by the small peaks, which should be ascribed to the combination of Cr atom and S radical in the reaction (discussed below). Thus, the major reaction formula in the process is proposed as follows. The carbon diffraction peak is absent because of its poor crystallinity. However, the Raman spectrum clearly shows the typical D- and G-band of carbon materials. Compared to the G-band, the D-band is broad and strong, suggesting the carbon shell is amorphous (Fig. 1(b)).[17]

$$(C_5H_5)_2Cr + (NH_4)_2S_2O_8 \rightarrow$$
$$C + Cr_2O_3 + Cr_2S_3 + (NH_4)_2SO_4 + SO_2 + H_2O.$$

The SEM image in Fig. 2(a) reveals that the powder comprises of homogeneous nanoparticles. In the high magnification image (Fig. 2(b)), the semitransparent carbon layer and the white inner cores beneath can be found, corresponding to the core–shell structure. However, these nanocrystals are encapsulated together rather than individually. This area can be further revealed in the backscattered electron (BSE) image (Fig. 2(c)), the equiaxed Cr_2O_3 nanocrystals with high atomic number contrast are evidently acquired, and the diameter of most nanocrystals is less than 100 nm. However, apart from the core–shell structure, a few large irregular shaped carbonaceous particles appear in the powder (Fig. 2(d)), which should be formed upon some side reaction.

From the TEM image in Fig. 3(a), the large spherical particles (black arrows) with a diameter of 60–100 nm and the agglomerated small nanocrystals (white arrows) are both completely encapsulated by the carbon shell without any

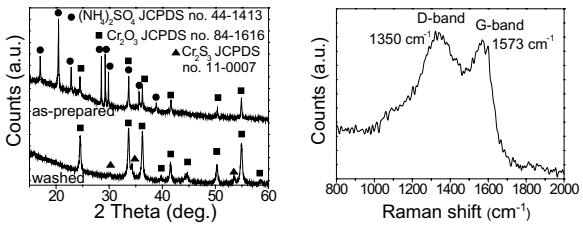

(a) (b)

Fig. 1. XRD patterns (a) and Raman spectrum (b) of the Cr_2O_3@C.

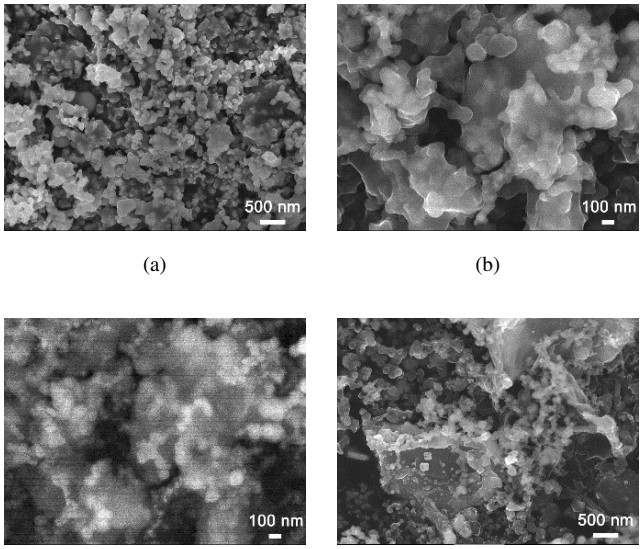

Fig. 2. SEM images of the Cr_2O_3@C: (a) low magnification, (b) high magnification, (c) BSE image of the same area of (b), (d) with some large irregular shaped particles at low magnification.

uncovered ones. The EDS spectrum of the large particle indicates that C, O, and Cr are the major elements with the O/Cr molar ratio close to the Cr_2O_3 stoichiometry (Fig. 3(f)). The trace of sulfur can be ascribed to its dissolution in the Cr_2O_3 nanocrystals. The HRTEM image shows that the small nanocrystals are tightly encapsulated by the carbon layer as a whole (Fig. 3(b)). The carbon shell is amorphous according to its disordered fringes and the small nanocrystal can be perfectly indexed to the Cr_2O_3 phase (Figs. 3(c) and 3(d)). The size distribution histogram displays that the diameter of Cr_2O_3 nanocrystals mainly ranges from 5 to 20 nm with a median size of 17 nm (Fig. 3(e)). The small Cr_2S_3 nanocrystals encapsulated by the carbon shell can also be found in HRTEM image (Supplementary data, Fig. S1). These results demonstrate that the method is very effective for the generation of core–shell structure with quite small inner cores.

The obvious weight loss of the Cr_2O_3@C in air initiates at 416°C, taken as the onset point of the TG curve, which corresponds to the oxidation of the 60 wt.% carbon shells (Fig. 4(a)). The phase composition of Cr_2O_3@C is directionally dependent on the Cr/C molar ratio in the Cp_2Cr. Given the high carbon atoms amount in the two Cp ligands, the weight percentage of carbon shell is calculated to be 61% in the nanocomposite. The reaction behavior of the reactants is shown in Fig. 4(b). The endothermic transition located at 169°C coincides with the melt of chromocene. However, the melting peak is not very sharp, and the gradual weight loss from 150°C is also observed in the TG curve. Therefore, a small quantity of chromocene has already participated in a reaction, because it has been proved that metallocene can

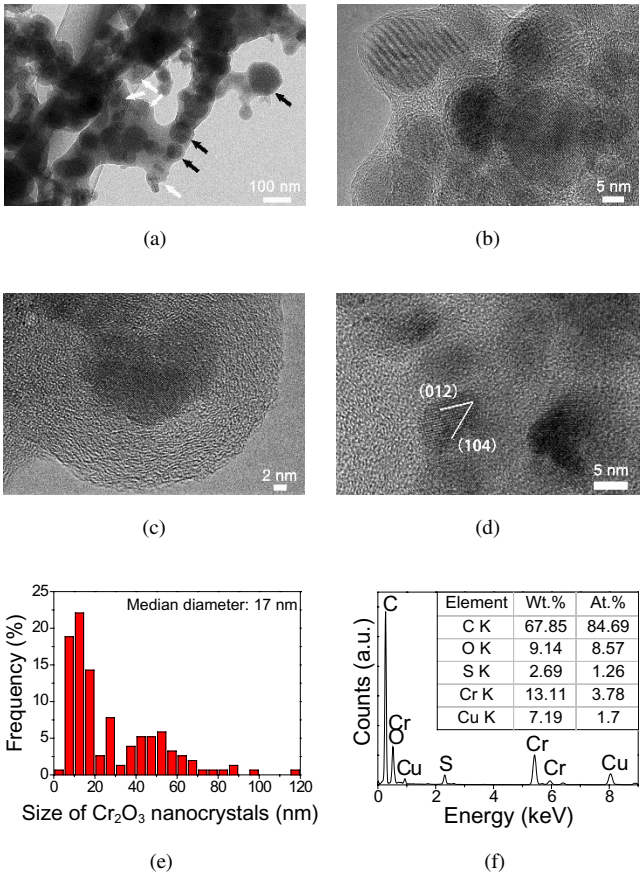

Element	Wt.%	At.%
C K	67.85	84.69
O K	9.14	8.57
S K	2.69	1.26
Cr K	13.11	3.78
Cu K	7.19	1.7

Fig. 3. (a) Large domain TEM image of the Cr_2O_3@C. HRTEM images of the Cr_2O_3@C (b), amorphous carbon shell (c) and lattice fringes of an individual Cr_2O_3 nanocrystal. (e) The size distribution of Cr_2O_3 nanocrystals. (f) EDS spectrum of the Cr_2O_3@C.

react with ammonium salt in an oxidizing environment to form carbon particles.[18] Actually, the major oxidation reaction takes place at 178°C according to the strongly exothermic peak with a 27% linear decrease in the TG curve, illustrating that this ultrafast reaction releases large amounts of heat and gaseous products, which can be regarded as an explosive reaction. This is the essence of the simple and efficient synthesis procedure.

The schematic of the synthesis process is shown in Fig. 5. Chromocene is one of the stable metallocene complexes and has a sandwich structure with Cp ligands bound to the central

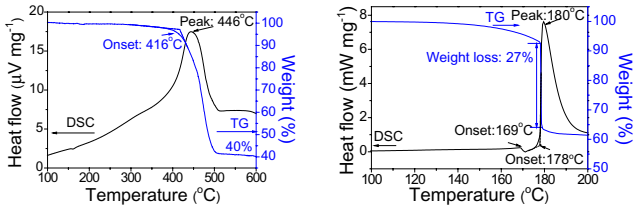

Fig. 4. DSC-TG curves of the Cr_2O_3@C (a) and the reactants (b).

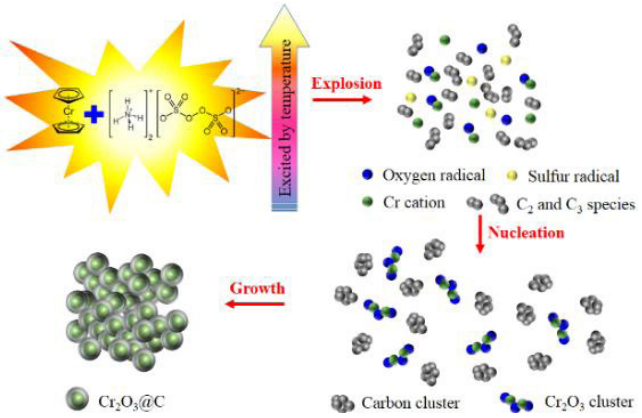

Fig. 5. The schematic of the synthesis process.

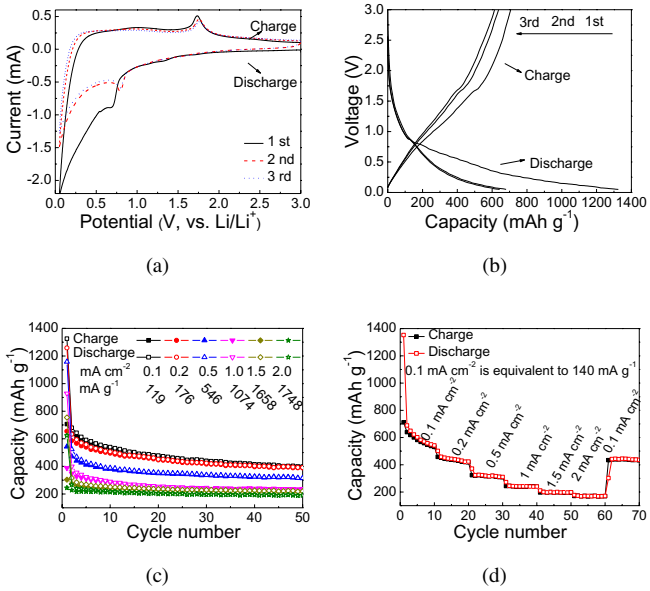

Fig. 6. Electrochemical properties of the Cr_2O_3@C: (a) CV; (b) The charge/discharge curves at a current density of 119 mA g^{-1}; (c) Cycling performance at different current densities; (d) Rate performance.

Cr atom. When its structure becomes unstable with the increase of temperature, the dissociated Cp radical will be very reactive toward the strong oxidizing agent. The H atoms in the Cp ring are suddenly oxidized to H_2O, resulting in an explosive reaction. Substantial energy is liberated during the process, by which the five-membered Cp rings are cleaved into C_2/C_3 carbon species, and the Cr atoms are oxidized to Cr_2O_3 clusters. Then, the nucleation and growth stage take place in sequence in a very short time, leading to the formation of very small Cr_2O_3 nanocrystals. In addition, the abundant carbon species also serve as a barrier to prevent the nanocrystals from getting together, eventually forming the carbon shell and the entirely encapsulated inner cores. Although the Cr atom is more inclined to bond with O radical, S radical also forms simultaneously in the violent reaction, leading to the formation of Cr_2S_3 nanocrystals. As a result, the reactants are required to closely contact with each other and can be regarded as an explosive, which will be excited by rising temperature. The yield is apparently related to the quantities of the reactants and can be easily scaled up in a larger autoclave.

Figure 6(a) presents the first three CV curves of Cr_2O_3@C. The broad reduction peak at ca. 0.7 V in the first cycle corresponds to the formation of SEI film. In the subsequent cycles, the curves almost overlap with a pronounced redox couple located at 0.8/1.8 V. In general, Cr_2O_3 phase does not have obvious CV peaks due to the amorphous nature of the product after conversion reaction.[13] Hence, these peaks are probably assigned to the lithiation/delithiation of the Cr_2S_3. Figure 6(b) shows the charge/discharge profiles of the Cr_2O_3@C. In the first cycle, the discharge and charge capacity are 1325 and 706 mAh g^{-1}, respectively. The irreversible capacity loss reaches as high as 47%, owing to the large quantities of amorphous carbon shell as well as the mass formation of SEI film on the Cr_2O_3@C with large surface area (Fig. S2). After the first cycle, the capacity slightly decreases and tends to be stable. The plateau at 0.8 and 1.8 V are not evident because the sulfur content is very low according to the EDS analysis. The major reaction is: $Cr_2O_3+6Li\leftrightarrow 2Cr+3Li_2O$. The cycling performance of the Cr_2O_3@C at different current densities are revealed in Fig. 6 (c) (The enlarged image is shown in Fig. S3). In comparison to the commercial bare Cr_2O_3,[19] the Cr_2O_3@C anode exhibits a good cyclic retention at 0.1 mA cm^{-2} (119 mA g^{-1}) and retains a reversible capacity of 397 mAh g^{-1} after 50 cycles. At higher current densities, a reversible capacity of 389, 313, 229, 222 and 193 mAh g^{-1} after 50 cycles is achieved at 0.2, 0.5, 1.0, 1.5 and 2.0 mA cm^{-2} (1748 mA g^{-1}), respectively. Moreover, the Cr_2O_3@C anode also has a good cycling stability at stepwise increased current densities (ranging from 140 to 2800 mA g^{-1}) every 10 cycles (Fig. 6(d)). It delivers a reversible capacity of 170 mAh g^{-1} in the 60th cycle and returns to 442 mAh g^{-1} at once when the current density changes from 1.2 to 0.1 mA cm^{-2}. Thus, the carbon encapsulation remarkably improves the cycling stability and rate capability of bare Cr_2O_3. However, the Cr_2O_3 composition in the nanocomposite should be further increased by using the organometallic precursor with a lower C/Cr molar ratio in order to achieve a higher capacity.

In conclusion, the explosive reaction between Cp_2Cr and $(NH_4)_2S_2O_8$ in an autoclave is decisive for the *in-situ* formation of Cr_2O_3@C. The one-step synthesis process is very simple, efficient and scalable, which is attractive for industrial applications. The carbon encapsulation improves the cycling stability and rate performance of the Cr_2O_3 anode.

Acknowledgments

The work is supported by National Natural Science Foundation of China (11572326), Natural Science Foundation of Shanghai (14ZR1419400) and Opening Fund of State Key Laboratory of Nonlinear Mechanics.

References

1. L. Lu *et al.*, *J. Power Sources* **226**, 272 (2013).
2. L. Ji *et al.*, *Energ. Environ. Sci.* **4**, 2682 (2011).
3. Z. Wang and L. Zhou, *Adv. Mater.* **24**, 1903 (2012).
4. Y. Wang *et al.*, *Nanoscale* **2**, 1294 (2010).
5. B. Liu *et al.*, *J. Nanopart. Res.* **18**, 375 (2016).
6. J. Liu *et al.*, *Chem. Commun.* **46**, 1437 (2010).
7. C. Nan *et al.*, *J. Am. Chem. Soc.* **136**, 4659 (2014).
8. W. Wang *et al.*, *ACS Appl. Mater. Interfaces* **5**, 6478 (2013).
9. J. Zheng *et al.*, *Nanotechnology* **23**, 165601 (2012).
10. B. Liu *et al.*, *Carbon* **68**, 573 (2014).
11. B. Liu *et al.*, *Nanotechnology* **27**, 075603 (2016).
12. B. Liu *et al.*, *Nanotechnology* **28**, 325603 (2017).
13. B. Guo *et al.*, *J. Power Sources* **205**, 495 (2012).
14. J. Hu *et al.*, *Electrochem. Solid-State Lett.* **8**, A66 (2005).
15. W. Yue *et al.*, *Carbon* **65**, 97 (2013).
16. B. Liu *et al.*, *Carbon* **127**, 21 (2018).
17. X. Xiang *et al.*, *Appl. Clay. Sci.* **42**, 405 (2009).
18. B. Liu *et al.*, *Carbon* **45**, 1710 (2007).
19. X. Zhao *et al.*, *J. Electrochem. Soc.* **162**, A1156 (2015).